Supporting information

Non-Covalent Planarizing Interactions Yield Highly Ordered and Thermotropic Liquid Crystalline Conjugated Polymers

Authors: Sina Sabury,[1,a] Zhuang Xu,[3,a] Shamil Saiev,[2] Daniel Davies,[3] Anna M. Österholm,[1] Joshua M. Rinehart,[1] Motahhare Mirhosseini,[4] Benedict Tong,[1] Sanggyun Kim,[5] Juan-Pablo Correa-Baena,[5] Veaceslav Coropceanu,[3] Oana D. Jurchescu,[4] Jean-Luc Brédas,[2] Ying Diao,[3] John R. Reynolds[1, *]

Affiliations:

[a]These authors contributed equally to this work

[1]School of Chemistry and Biochemistry, School of Materials Science and Engineering, Center for Organic Photonics and Electronics, Georgia Tech Polymer Network, Georgia Institute of Technology, Atlanta, Georgia 30332, United States.

[3]Department of Chemistry and Biochemistry, The University of Arizona, Tucson, AZ 85721-0041, United States

[3]Department of Chemical and Biomolecular Engineering, Department of Chemistry, Beckman Institute for Advanced Science and Technology, University of Illinois Urbana−Champaign, 600 S. Mathews Avenue, Urbana, Illinois 61801, United States

[4]Department of Physics and Center for Functional Materials, Wake Forest University, Winston-Salem, NC 27109 United States

[5]School of Materials Science and Engineering, Georgia Institute of Technology, Atlanta, Georgia 30332, United States

Table of Contents

Computational methodology

Ab-initio calculations

All DFT calculations were conducted at the M06-2X/6-311G** level of theory using the Gaussian 16 package.[1] The dihedral angle between the studied groups were fixed from 0° to 360° at 10° intervals and geometry optimization was performed on all remaining degrees of freedom.

Molecular dynamics simulations

All-atom (AA) molecular dynamics (MD) simulations were performed using the LAMMPS package[2] and the Optimized Potentials for Liquid Simulations−All Atom (OPLS-AA) force field (see Figure S1 for dihedral scan of phenylenethienylene and thienylene-thienothiophene using optimized OPLS-AA Force Field).[3] Atom types and parameters were defined using the LigParGen web server.[4] For the phenylene-thienylene and thienylene-thienothiophene dihedrals the force-field parameters were optimized based on results obtained from DFT calculations, the results are shown in Figure S1 and optimized 13 coefficients for each dihedral are listed in Table S1. Atomic partial charges were determined by fitting the DFT-determined electrostatic potential (CM5) at the M06-2X/6-311G** level of theory.[5] Long-range electrostatic interactions of charged particles were computed using the particle-particle-particle-mesh (PPPM) algorithm with a root-mean-accuracy of 10^{-5}.[6] The Verlet integrator with a time step of 1 fs was used, and the Nose−Hoover thermostat/barostat was employed for temperature/pressure control. All related simulations were performed using either NVT (constant Number of particles, Volume, and

Temperature) or NPT (constant number of molecules, pressure, and temperature) ensembles at pressure of 1 atm. A cutoff of 12 Å was applied for the summation of van der Waals interactions.

Table S1. OPLS-AA Optimized Force Field Parameters for Phenylene-Thienylene and Thienylene-Thienothiophene Dihedrals (13 Parameters Each)

	Phenylene-Thienylene	**Thienylene-Thienothiophene**
A	2.99494	1.5716
B	1.11645	-0.14649
C	-8.91671	-4.97007
D	-10.86306	-13.663
E	-1.88687	-11.89236
F	48.13495	59.19301
G	4.03606	88.66136
H	-70.29769	-108.79631
I	4.69402	-234.6759
J	41.2865	95.83407
K	-11.05188	258.03093
L	-7.25643	-32.45405
M	3.40924	-101.0592

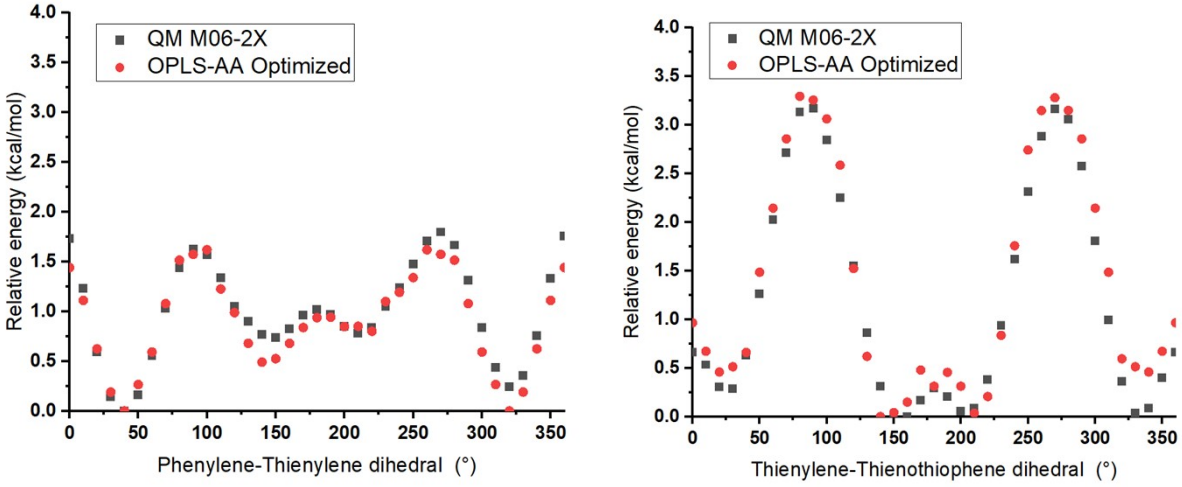

Figure S1. Dihedral scan of phenylenethienylene and thienylene-thienothiophene using optimized OPLS-AA Force Field and comparison with DFT Results.

To examine the aggregation dynamics of TPT-TT polymers in toluene and chlorobenzene, we conducted NPT simulations using trimer pair chains placed in both solvents at 15 mg/ml, across a temperature range of 270 to 330K. Simulations ran for 150 ns or until the centers of mass separated by 20 Å, a criterion established to indicate irreversible separation. This is to observe if the two trimers either separate or display a tendency to dissociate at different temperatures, thus offering insights into the solvation behavior of this polymer. Figure S2 depicts the separation distance in relation to temperature for both solvents, showing a more pronounced separation in chlorobenzene, with distinct occurrence at room temperature. However, the chains in toluene maintained their association throughout the simulation, with only a slight increase in separation distance observed at 330 K. Since MD simulations operate on a different timescale compared to experiment, the lack of chain dissociation should not be viewed as an inherent characteristic of

polymer aggregation, rather it serves as an indicator permitting a comparative assessment of polymer solubility within the investigated solvents.

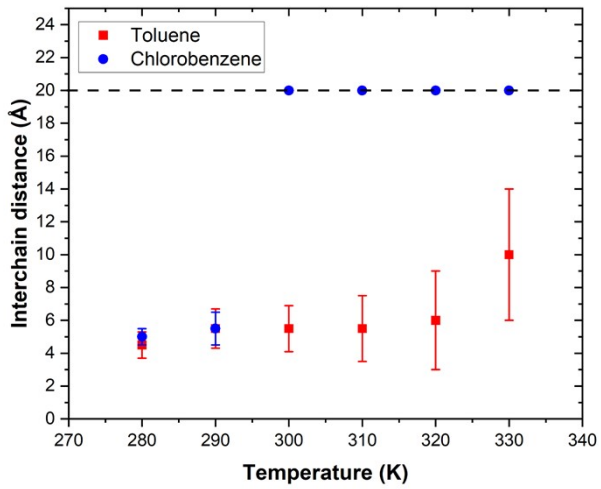

Figure S2. Temperature-dependent TPT-TT trimer chain separation in chlorobenzene and toluene.

Synthesis of intermediate molecules and TPT-TT monomer

All starting materials were purchased from a commercial supplier and were used without further purification. The synthesis pathway for TPT-TT (see Figure S3), synthesis details of intermediate molecules, and the dibromo monomer are presented in the following section. Molecule 2 (2-(4-decylthiophen-2-yl)-4,4,5,5-tetramethyl-1,3,2-dioxaborolane) is synthesized following a procedure from literature.[7]

^{1}H NMR and ^{13}C NMR spectra for all monomers and molecular precursors were acquired on a Bruker Avance IIIHD 500 MHz or Bruker Avance IIIHD 700 MHz instruments using $CDCl_3$ as solvent; the residual $CHCl_3$ peak was used as a reference for all reported chemical shifts (^{1}H:

δ= 7.26 ppm, ^{13}C: δ= 77.16 ppm). Mass spectrometry of small molecules was obtained by direct infusion atmospheric pressure chemical ionization (APCI) in positive mode using a Thermo Scientific Orbitrap ID-X Tribrid mass spectrometer. Gel permeation chromatography (GPC) was performed using a Tosoh EcoSEC high temperature GPC instrument at the Organic Materials Characterization Laboratory (OMCL) at Georgia Tech with RI detector to determine the number average molecular weight (M_n), weight average molecular weight (M_w) and dispersity ($Đ$). Experiments were run using 1,2,4-trichlorobenzene (TCB) as the eluent at 140 °C at a flow rate of 1 mL/min on two 7.8 mm x 30 cm, 13 μm TSK-Gel GMHHR-H(S) HT2 columns in series. The instrument was calibrated using polystyrene standards (1,390-1,214,000 g/mol) and the data were analyzed using 8321GPC-WS analysis software. The GPC samples were prepared by dissolving the polymers in TCB at a 1 mg/mL concentration and stirred at 120 °C for at least 3 hours before filtering through a 0.45 μm PTFE filter. Elemental analyses were conducted by Atlantic Microlab Inc. The MALDI-TOF mass spectra were performed at the Georgia Institute of Technology Bioanalytical Mass Spectrometry Facility with a Bruker Autoflex 111. The matrix substance used for all MALDI samples was trans-2-[3-(4-tert-Butylphenyl)-2-methyl-2-propenylidene]malononitrile (DCTB).

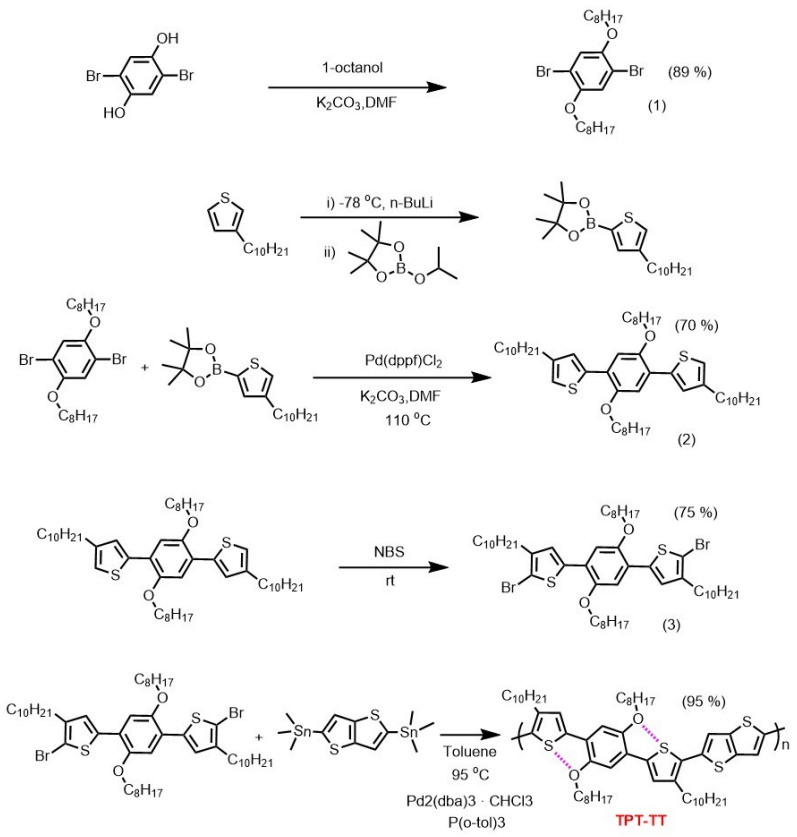

Figure S3. Synthesis pathway for TPT-TT. Yields are shown in parentheses.

Synthesis of 1,4-dibromo-2,5-bis(octyloxy)benzene (1)

Similar to a reported procedure,[8] 50 mL of dry dimethylformamide (DMF) and 2,5-dibromohydroquinone (811 mg, 3.02 mmol) were added to a pre-dried 250 mL round bottom flask equipped with a stir bar. Then, 1.32 mL (7.55 mmol, 2.5 equiv.) of 1-bromooctane was added followed by the addition of excess potassium carbonate (1.24 g, 3 equiv.). the reaction mixture was left to stir overnight (16 hours) at 90 °C. The solvent was removed under reduced pressure via rotary evaporation and the remaining contents were purified using silica gel plug (DCM as mobile solvent) followed by silica gel column chromatography with 2:1 ratio of hexane:dichloromethane

as mobile phase to afford a white powder (1.4 g, 89%). ^{1}H NMR (700 MHz, $CDCl_3$), δ(ppm): 7.08 (s, 1H), 3.94 (t, J = 6.5 Hz, 2H), 1.82-1.77 (m, 2H), 1.49-1.45 (m, 2H), 1.38-1.24 (m, 8H), 0.89 (t, J = 7.0 Hz, 3H). ^{13}C{^{1}H} NMR (176 MHz, $CDCl_3$), δ (ppm): 150.05, 118.44, 111.10, 70.29, 31.76, 29.23, 29.18, 29.08, 25.90, 22.63, 14.08. NMR spectra are consistent with a previous report and shown in Figure S4 and Figure S5.[9]

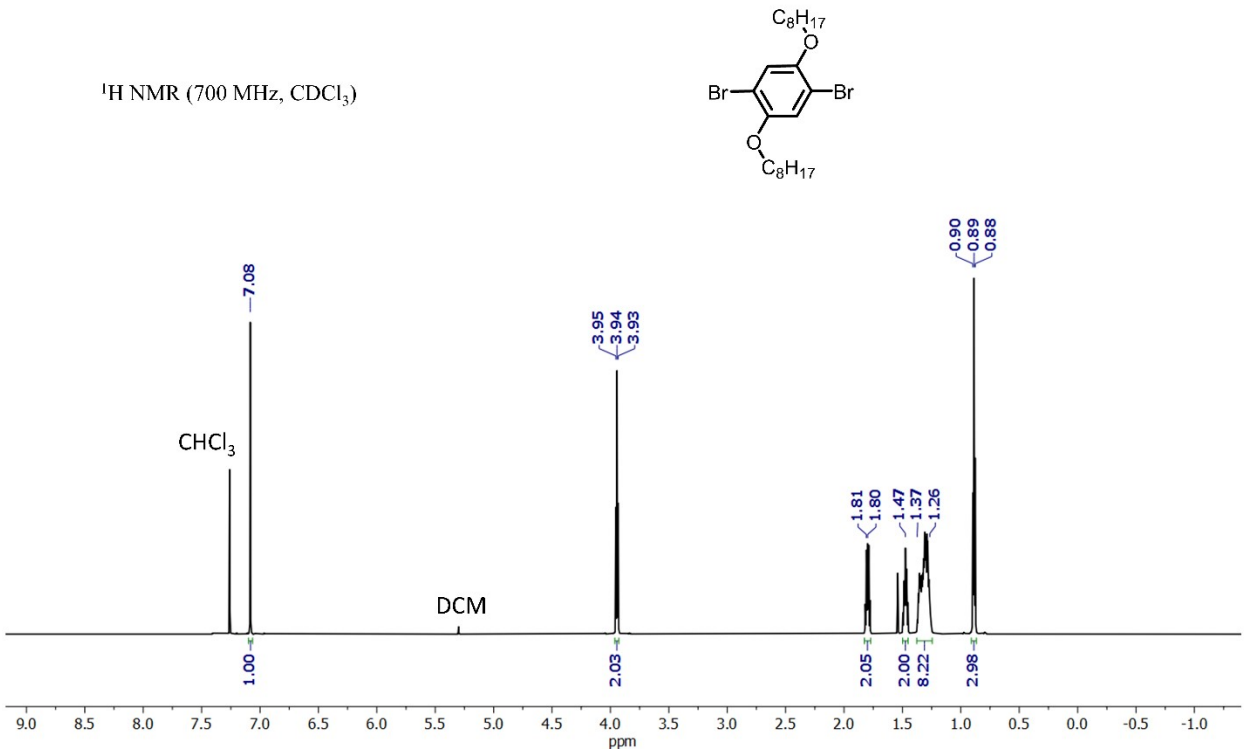

Figure S4. ^{1}H NMR of 1,4-dibromo-2,5-bis(octyloxy)benzene (1).

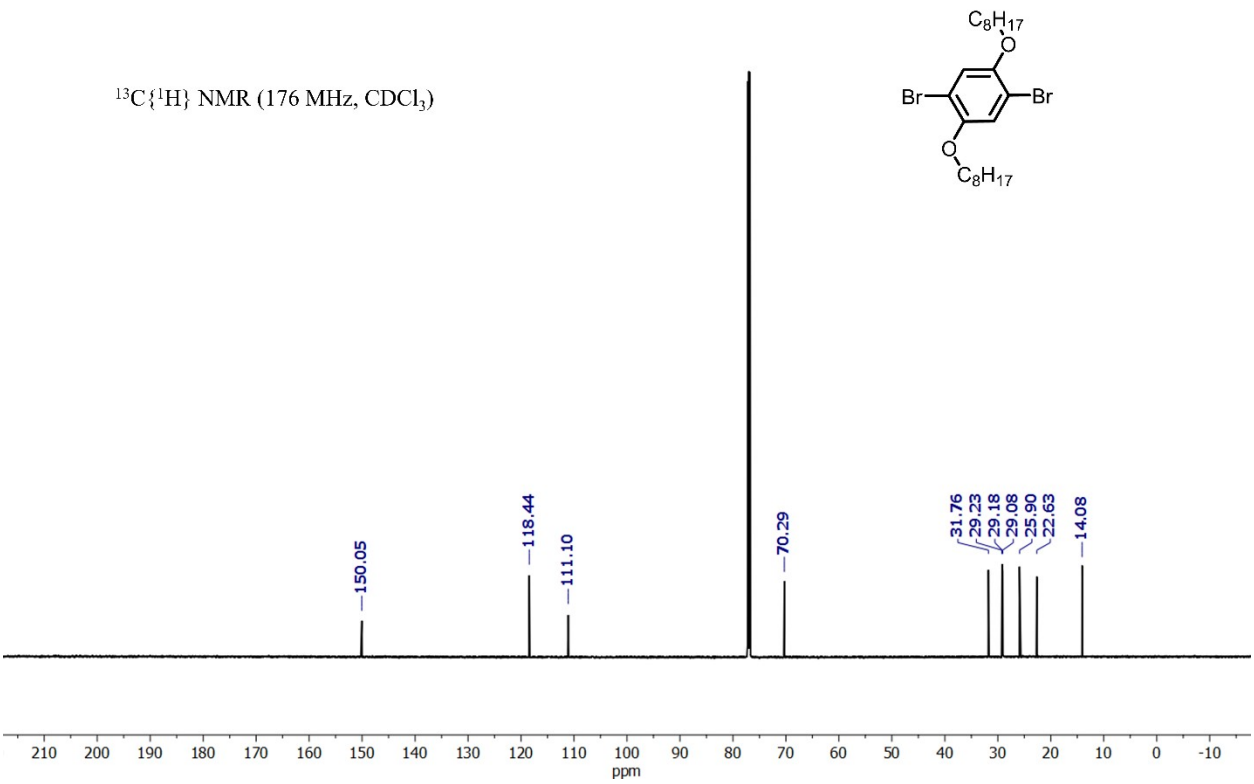

Figure S5. ^{13}C NMR of 1,4-dibromo-2,5-bis(octyloxy)benzene (1).

Synthesis of 5,5'-(2,5-bis(octyloxy)-1,4-phenylene)bis(3-decylthiophene) (3) (TPT core)

75 mL of dry dimethylformamide (DMF) and 1,4-dibromo-2,5-bis(octyloxy)benzene (1) (316 mg, 0.64 mmol) were added to a pre-dried 250 mL round bottom flask equipped with a stir bar. Then, 679 mg (1.86 mmol, 2.9 equiv.) of 2-(4-decylthiophen-2-yl)-4,4,5,5-tetramethyl-1,3,2-dioxaborolane (2) was added followed by the addition of 56 mg (0.1 equiv.) of [1,1′-bis(diphenylphosphino)ferrocene]palladium(II) dichloride dichloromethane adduct ($Pd(dppf)Cl_2 \cdot DCM$) as the catalyst. Excess potassium carbonate (309 mg, 3 equiv.) was added to the flask and the reaction mixture was left to stir overnight (16 hours) at 110 °C. The solvent was removed under reduced pressure via rotary evaporation and the remaining contents were purified using silica gel

plug (DCM as mobile solvent) followed by silica gel column chromatography with 4:1 ratio of hexane:dichloromethane as mobile phase to afford a white powder (350 mg, 70%). ^{1}H NMR (500 MHz, $CDCl_3$), δ(ppm): 7.38 (d, J = 1.4 Hz, 1H), 7.21 (s, 1H), 6.92 (d, J = 1.3 Hz, 1H), 4.07 (t, J = 6.4 Hz, 2H), 2.63 (t, J = 7.7 Hz, 2H), 1.93-1.86 (m, 2H), 1.70-1.62 (m, 2H), 1.57-1.51 (m, 2H), 1.39-1.24 (m, 22H), 0.91-0.86 (m, 6H). ^{13}C{^{1}H} NMR (126 MHz, $CDCl_3$), δ (ppm): 149.44, 143.14, 139.10, 126.92, 123.14, 120.48, 112.85, 69.81, 32.07, 32.00, 30.79, 30.73, 29.81, 29.69, 29.63, 29.58, 29.51, 29.43, 26.47, 22.84, 14.27 (see Figures S6 and S7). HR-MS (APCI) m/z for $C_{50}H_{82}O_2S_2$ theoretical (M+H): 779.5828, found (M+H): 779.5814.

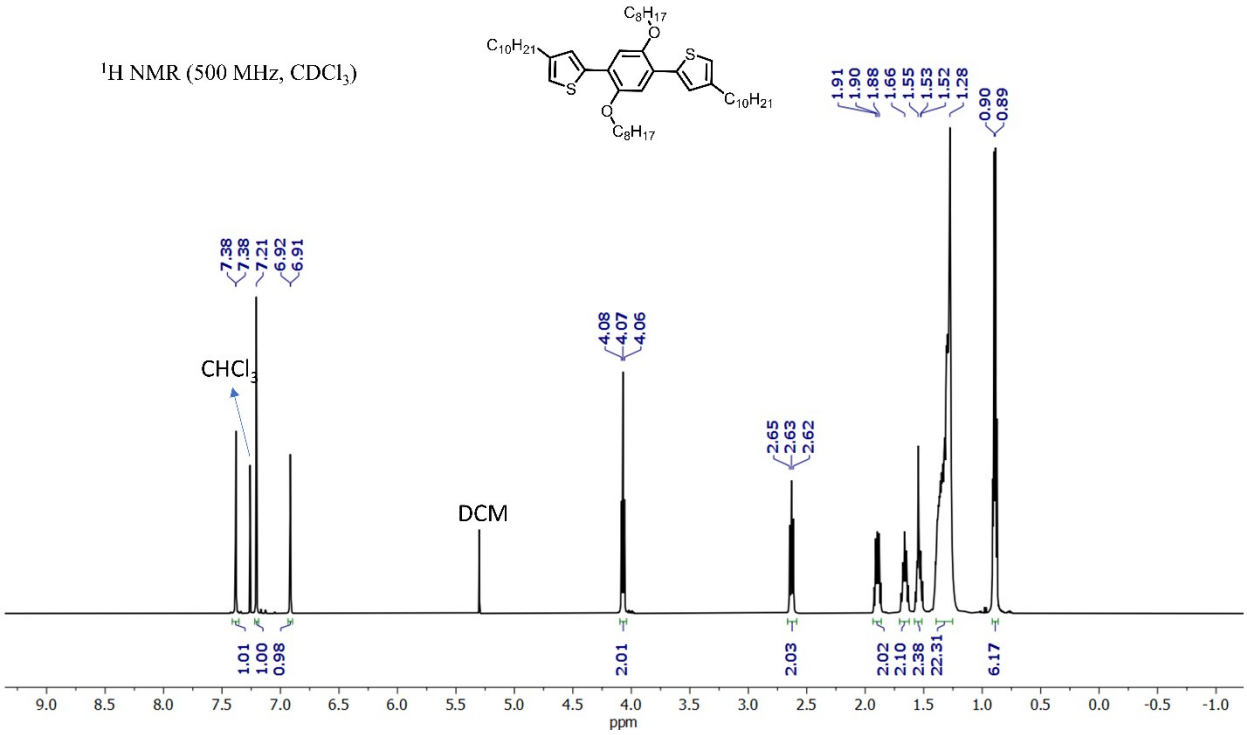

Figure S6. ^{1}H NMR of TPT core, 5,5'-(2,5-bis(octyloxy)-1,4-phenylene)bis(3-decylthiophene) (3).

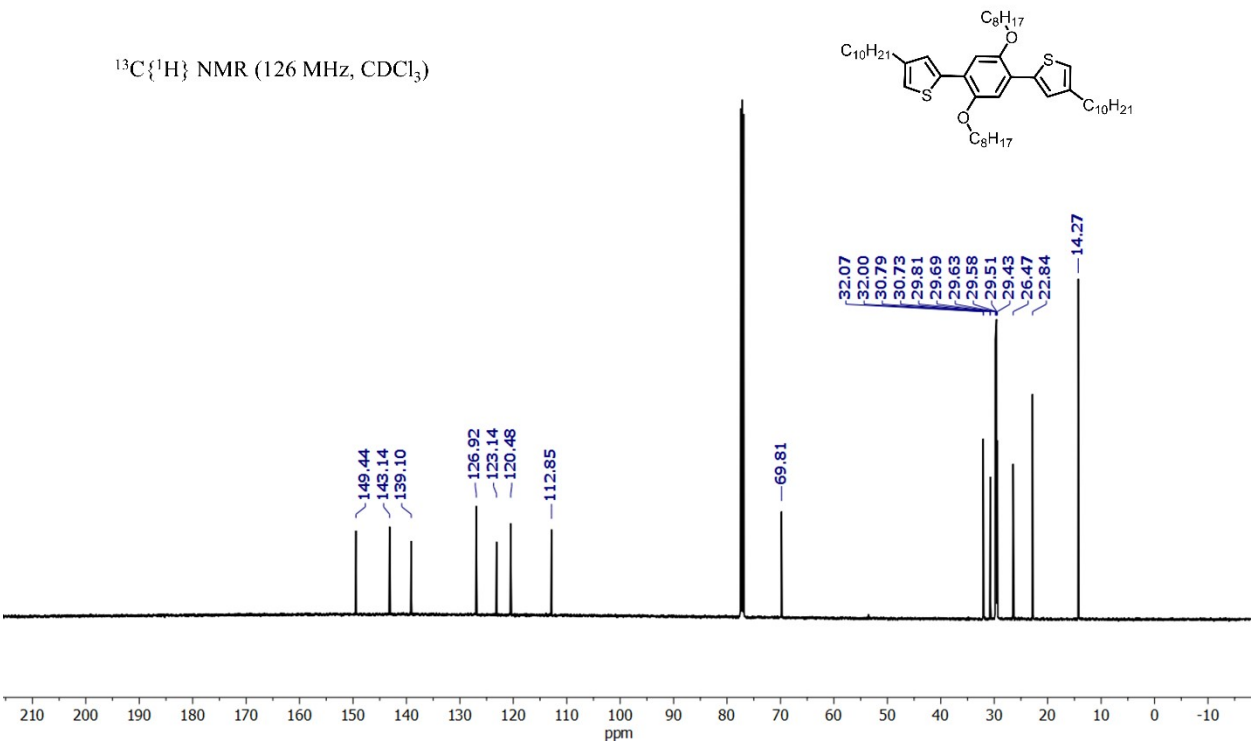

Figure S7. ^{13}C NMR of TPT core, 5,5'-(2,5-bis(octyloxy)-1,4-phenylene)bis(3-decylthiophene) (3).

Synthesis of 5,5'-(2,5-bis(octyloxy)-1,4-phenylene)bis(2-bromo-3-decylthiophene) (4) (dibromo TPT monomer)

320 mg of the molecule (3), 5,5'-(2,5-bis(octyloxy)-1,4-phenylene)bis(3-decylthiophene) (0.40 mmol) was added to a 250 mL round bottom flask, which had been pre-dried and equipped with a stir bar. Subsequently, 30 mL of chloroform was added. The resulting mixture was cooled to 0 °C using an ice bath. Next, 136 mg (0.78 mmol, 1.95 equiv.) of *N*-bromosuccinimide (NBS) was slowly added over a period of 10 minutes, and the reaction flask was covered from light. The reaction was then allowed to gradually return to room temperature by stopping the addition of ice to the bath. The product was extracted by using a mixture of dichloromethane (DCM) and water.

The organic layer was dried with Na_2SO_4, filtered, and concentrated under reduced pressure. The product was purified by silica gel column chromatography with 5:1 ratio of hexane:dichloromethane as mobile phase to afford a pale yellow powder (280 mg, 75%).^{1}H NMR (700 MHz, $CDCl_3$), δ(ppm): 7.20 (s, 1H), 7.12 (s, 1H), 4.07 (t, J = 6.5 Hz, 2H), 2.60 (t, J = 7.7 Hz, 2H), 1.93-1.88 (m, 2H), 1.71-1.63 (m, 2H), 1.57-1.52 (m, 2H), 1.39-1.24 (m, 22H), 0.91-0.86 (m, 6H) (see Figure S8).^{13}C{^{1}H} NMR (126 MHz, $CDCl_3$), δ (ppm): 149.25, 141.63, 138.44, 125.61, 122.57, 111.44, 110.17, 69.91, 32.07, 32.00, 30.04, 29.81, 29.79, 29.77, 29.64, 29.57, 29.54, 29.51, 29.50, 29.43, 26.46, 22.85, 14.28 (see Figure S9).

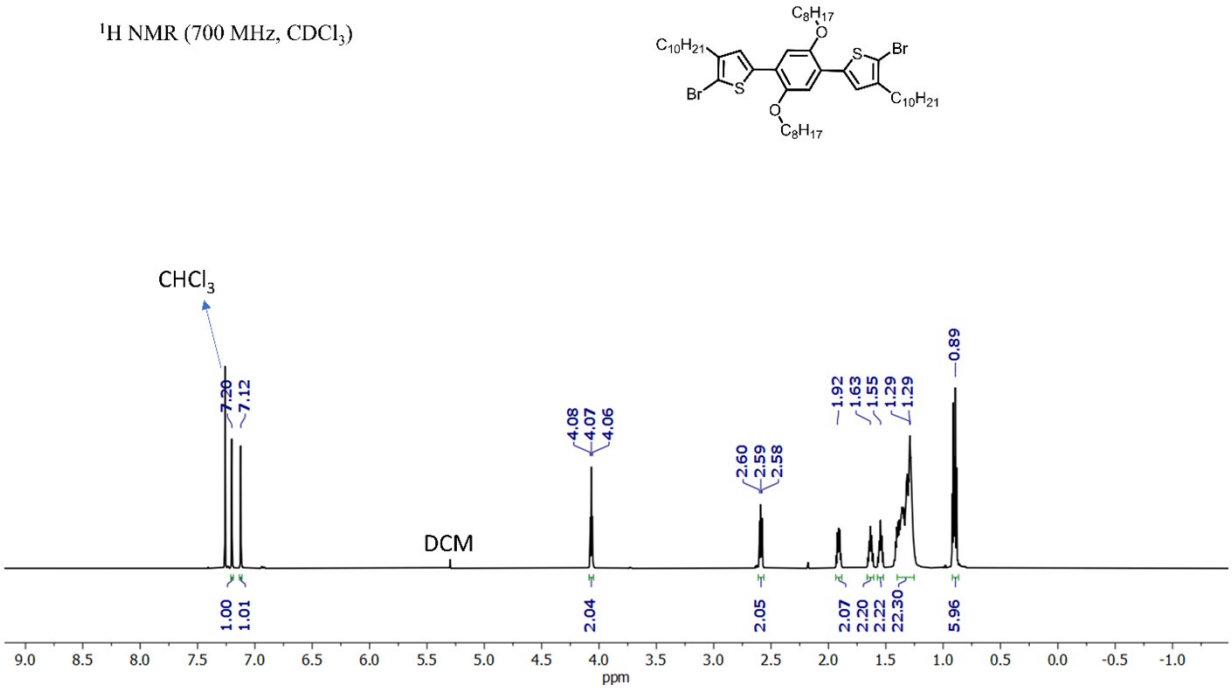

Figure S8. ^{1}H NMR of di bromo TPT comonomer, 5,5'-(2,5-bis(octyloxy)-1,4-phenylene)bis(2-bromo-3-decylthiophene) (4).

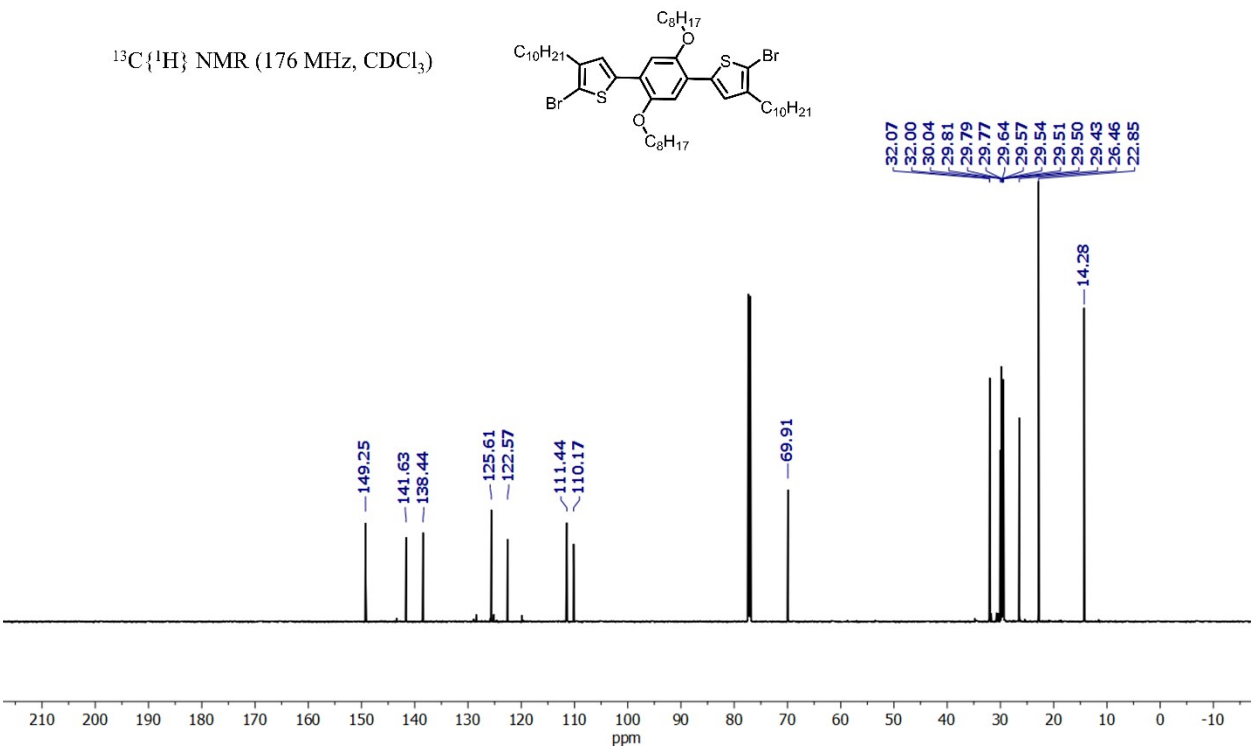

Figure S9. ^{13}C NMR of di bromo TPT comonomer, 5,5'-(2,5-bis(octyloxy)-1,4-phenylene)bis(2-bromo-3-decylthiophene) (4).

Polymerization procedure and general characterizations

2,5-bis(trimethylstannyl)thieno[3,2-b]thiophene (200 mg, 0.43 mmol, 1 equiv.) and dibromo TPT monomer (402 mg, 0.43 mmol, 1 equiv.) were added to a freshly dried and cooled round bottom flask equipped with a stir bar. Subsequently, the flask was transferred to a glove box where dipalladium-tris(dibenzylideneacetone)chloroform complex ($Pd_2(dba)_3 \cdot CHCl_3$) was added as the catalyst (21 mg, 0.021 mmol, 0.05 equiv.), along with tris(o-tolyl)phosphine as the ligand (26 mg, 0.086 mmol, 0.2 equiv.), and 4 mL of toluene as the polymerization solvent. The reaction flask was then removed from the glove box and immersed in an oil bath set at 105 °C, allowing it to stir for 16 hours at this temperature. After this time, a small amount of palladium scavenger

(diethylammonium diethyldithiocarbamate) was added, and the temperature was lowered to 90 °C. The solution was stirred for an additional hour at 90 °C, followed by cooling to room temperature. The crude polymer was precipitated by adding it to stirring cold methanol. Further purification of the crude polymer was achieved through Soxhlet washing with methanol (24 hours), acetone (24 hours), and hexane (24 hours). The purified polymer was obtained via Soxhlet extraction using chloroform. Subsequently, the purified polymer was reprecipitated into cold methanol and collected as a red solid by vacuum filtration on a nylon membrane with a pore size of 45 μm. The number-average molecular weight was 24.6 kg/mol and the dispersity (Đ) was 1.93 with a monomodal distribution as measures by GPC (Figure S11). MALDI-TOF was used to confirm equivalent incorporation of TPT and TT (Figure S12 and Figure S13). ^{1}H NMR (500 MHz, $CDCl_3$), δ(ppm): 7.44 (s, 1H), 7.30 (s, 1H), 7.24 (s, 1H), 4.15 (m, 2H), 2.85 (m, 2H), 1.99-1.90 (m, 2H), 1.78-1.68 (m, 2H), 1.68-1.51 (m, 2H), 1.42-1.26 (m, 22H), 0.90-0.86 (m, 6H) (see Figure S10). Anal. calcd. for $C_{56}H_{82}O_2S_4$: C (73.47%), S (14.01%), H (9.03%), O (3.50%); Found: C (72.84%), S (14.40%), H (9.02%).

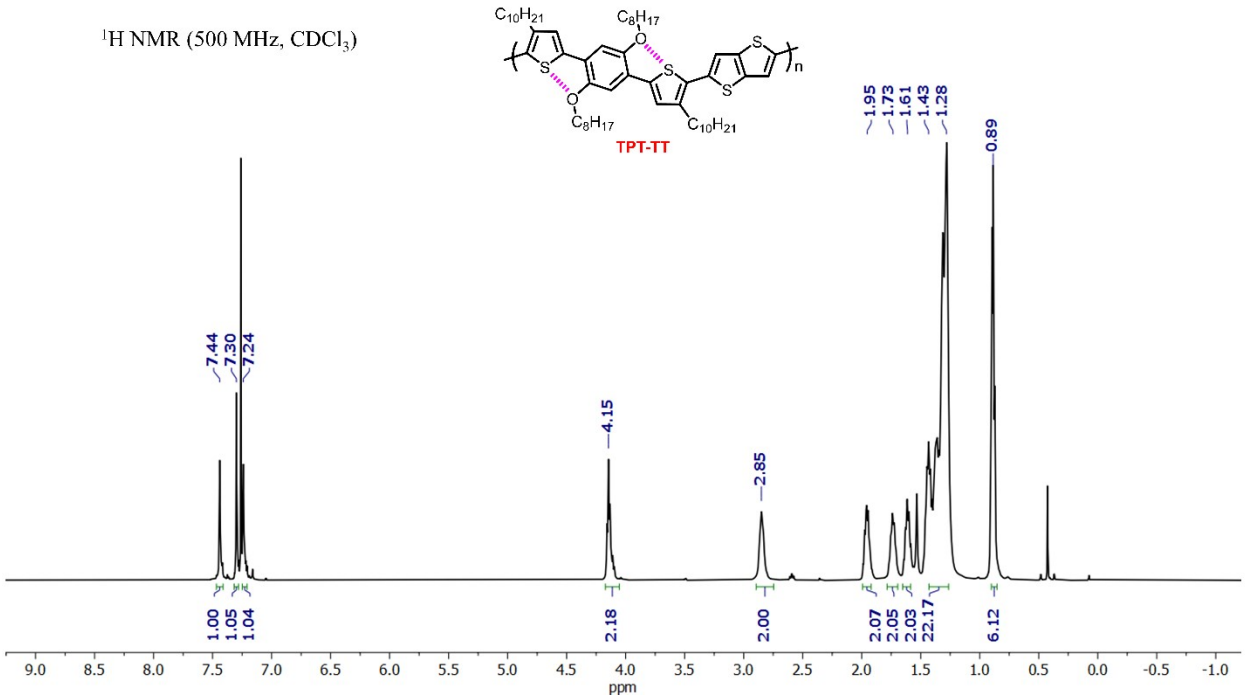

Figure S10. ^{1}H NMR of TPT-TT in $CDCl_3$ at room temperature.

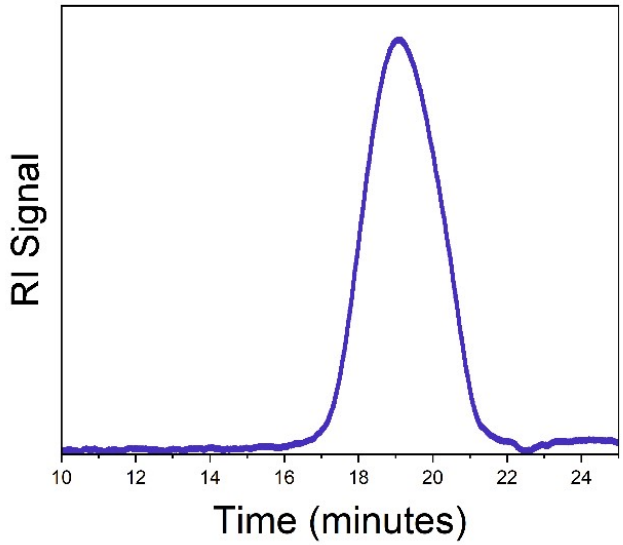

Figure S11. High temperature (140 °C) GPC trace of TPT-TT dissolved in trichlorobenzene (M_n = 24.6 kg/mol, Đ = 1.93).

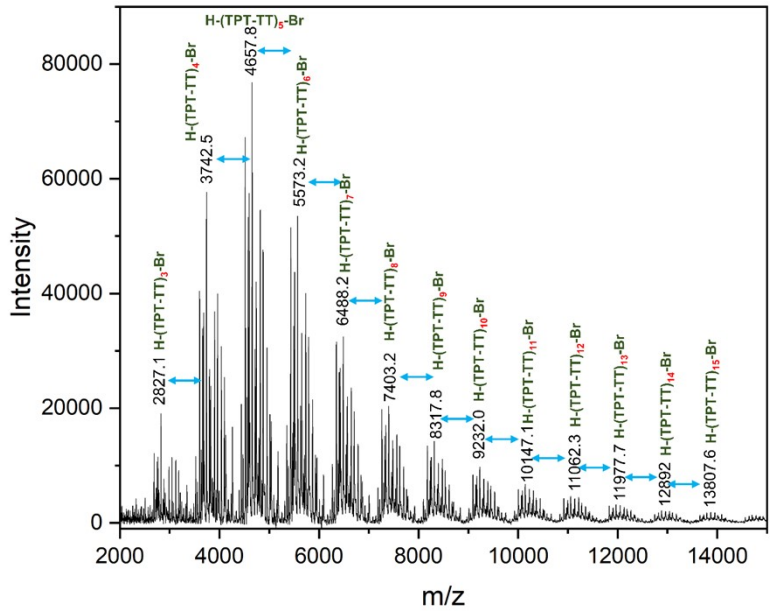

Figure S12. MALDI-TOF spectrum of TPT-TT. The mass to charge (m/z) peaks are separated by the mass of the TPT-TT unit.

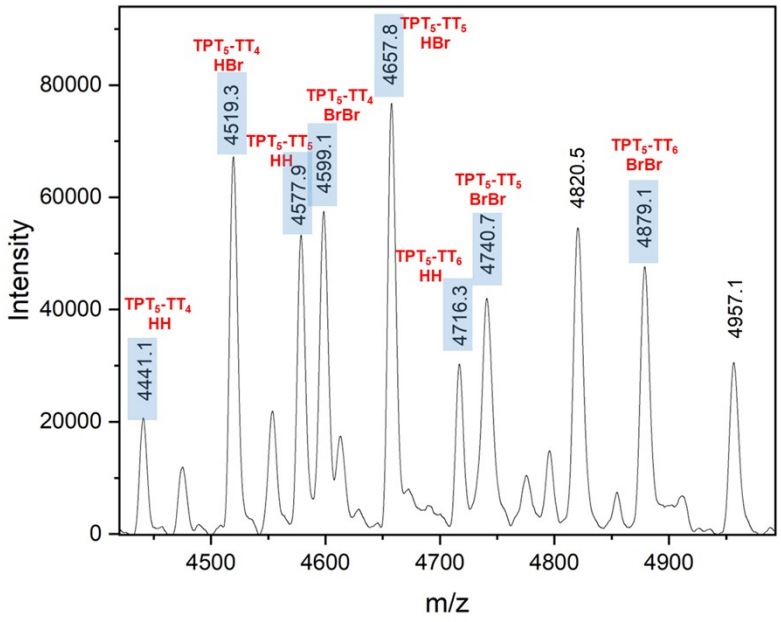

Figure 13. End group analysis for TPT-TT in the mass to charge (m/z) range of 4400-5000 based on the MALDI-TOF spectrum. Identified mass to charge numbers show that chains are mostly terminated by HBr end groups followed by HH and BrBr for TPT_5-TT_5, respectively. TPT:TT

incorporation is considered equivalent. Deviation form 1:1 in observed species of TPT_5-TT_4 and TPT_5-TT_6 are related to the end units. Higher offset would be indicative of possible homocoupling which is not observed here.

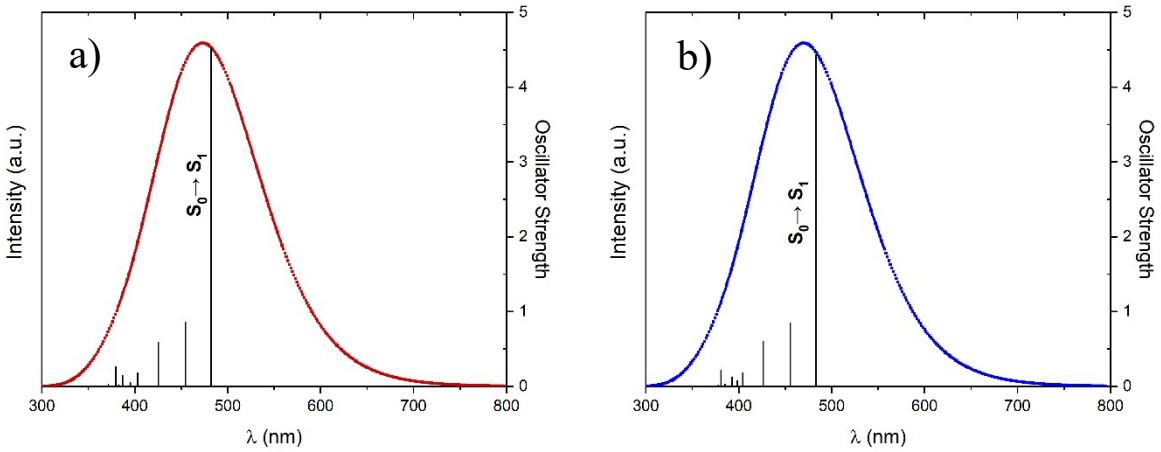

Figure S14. Computationally estimated UV-vis absorption spectra of TPT-TT in (a) toluene and (b) chlorobenzene. The main absorption feature is determined to be predominantly due to the $S_0 \rightarrow S_1$ electronic transition at λ = 482 nm (2.56 eV).

Thermal stability measurements

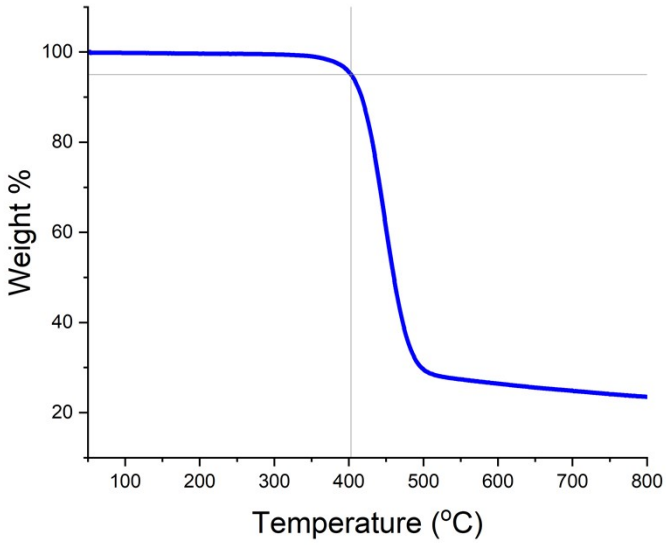

Figure S15. Thermogravimetric analysis of TPT-TT ramping from 50 °C to 800 °C at a rate of 20 °C/min under nitrogen environment. TPT-TT is thermally stable, and the onset of the decomposition process (405 °C at 5 % weight loss) is well above the thermal transitions observed in the DSC.

Thermotropic liquid crystallinity and morphology

In-situ CPOM and GIXD images

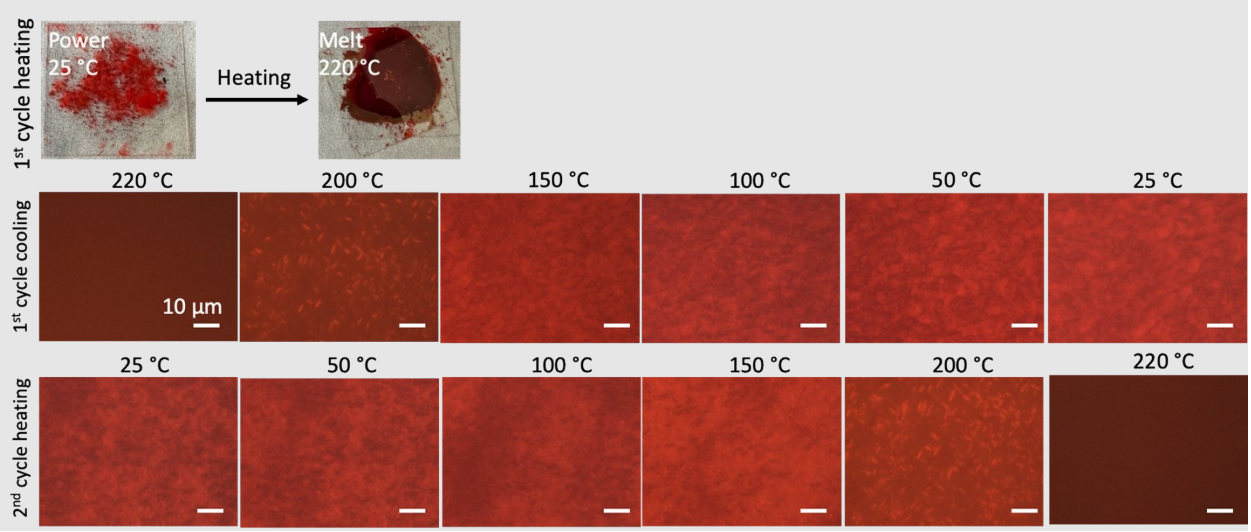

Figure S16. Heating and cooling processes of TPT-TT powder sandwiched between two glass slides. The powder at 25 °C was heated to form a melt at 220 °C (first row). Cross-polarized optical images (CPOM) show the emergence of liquid crystalline phase upon cooling from the melt state (second row). CPOM images show the heating process in the second thermal cycle resulting in an isotropic phase at 220 °C (third row).

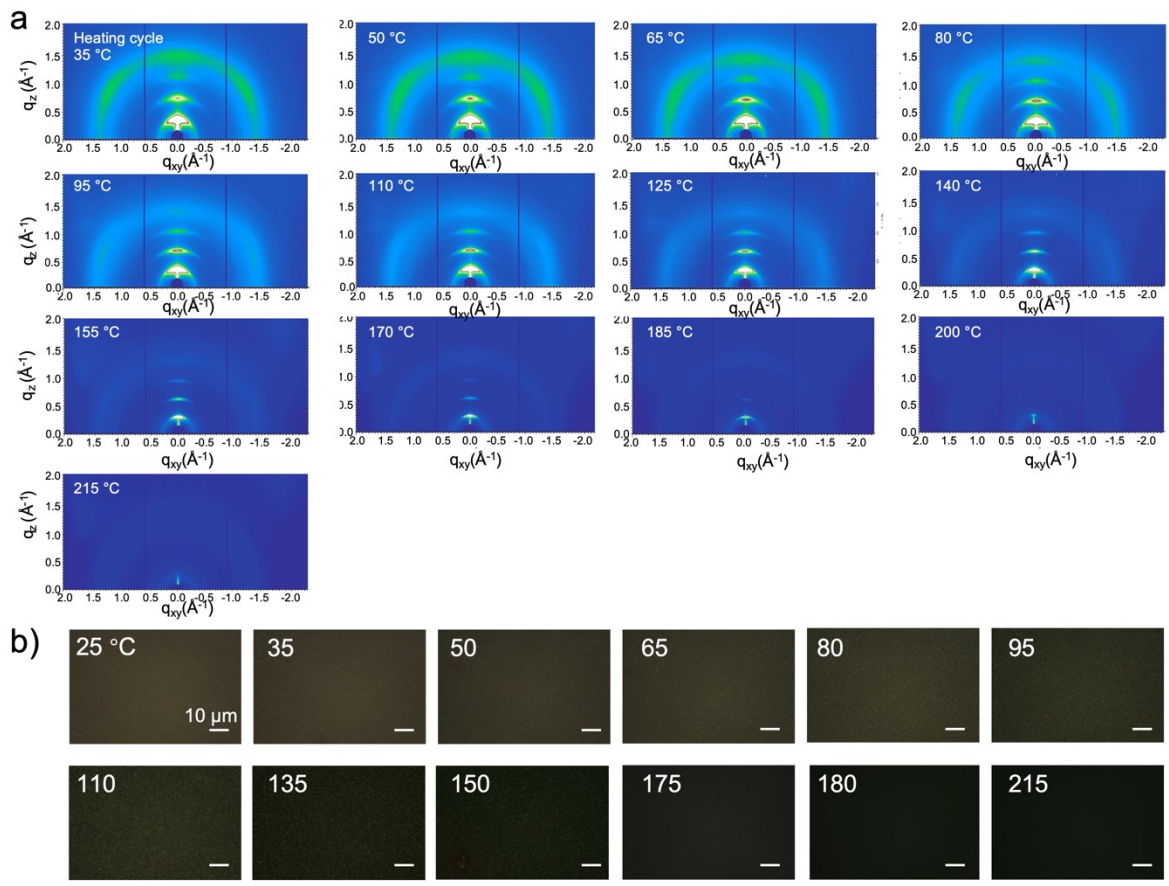

Figure S17. In-situ GIXD a) and CPOM b) images and of as-spun film during the first heating cycle.

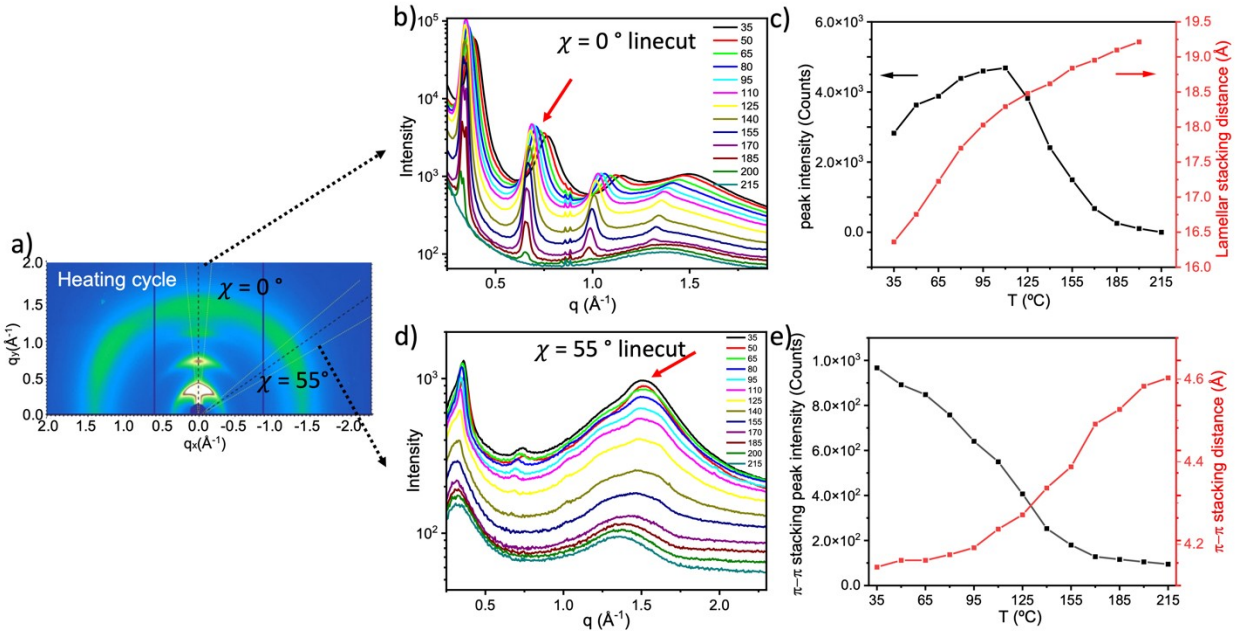

Figure S18. GIXD analysis and temperature-dependent structural changes. a) Representative GIXD image with linecut locations. b) Out-of-plane linecut at a 90° azimuthal angle across different temperatures. c) Variation of lamellar stacking distance and peak intensity with heating temperature. d) Linecut at a 35° azimuthal angle across different temperatures. e) Variation of π-π stacking distance and peak intensity with heating temperature.

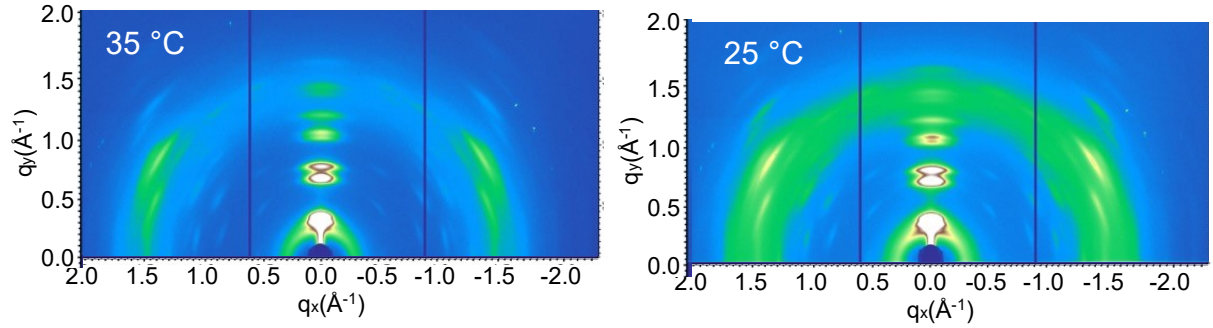

Figure S19. In-situ GIXD images during first cooling cycle at 35 °C and 25 °C.

CPOM and GIXD details

The films for CPOM measurements were prepared by spin-coating a 10 mg/mL chlorobenzene at 500 rpm onto a bare Si substrate. Subsequently, the films were relocated to a Linkam stage and the birefringence of the films was directly observed under CPOM throughout a thermal cycle. This involved heating the films above their melting temperature and subsequently cooling them down to room temperature at a rate of 10 °C/min.

The GIXD measurements on the films were carried out at the Advanced Photon Source at the Argonne National Laboratory, specifically on beamline 8-ID-E. An incident beam energy of 10.92 keV was utilized to gather the diffraction data via a 2D detector (PILATUS 1M). Measurements were taken at two distinct positions, with a sample-to-detector distance set at 217 mm. The samples were scanned under a helium environment with an exposure time of 10 seconds and an incidence angle of 0.14º. The unit cell for the annealed sample was obtained by fitting the calculated peak positions of the reciprocal lattice $\left\{q_{xy}^{calc},\ q_{z}^{calc}\right\} = \left\{kb_{\parallel}^{*} + lc_{\parallel}^{*}, h\left|a^{*}\right| + kb_{\perp}^{*} + lc_{\perp}^{*}\right\}$ to the experimentally measured peak positions. Here, the subscript $\parallel$ denotes the 2D in-plane reciprocal unit cell vectors (x,y-components), and $\perp$ the respective out-of-plane components. The best fit unit cells are obtained by looking for reciprocal basis vectors a^{*}, b^{*}, c^{*} for which the least square error $\sum_{peaks} = \left(\left|q_{xy}^{calc} - q_{xy}^{exp}\right| + \left|q_{z}^{calc} - q_{z}^{exp}\right|\right)^{2}$ is minimal. The fitted unit cell is reported with the b-c plane defined as parallel to the substrate.

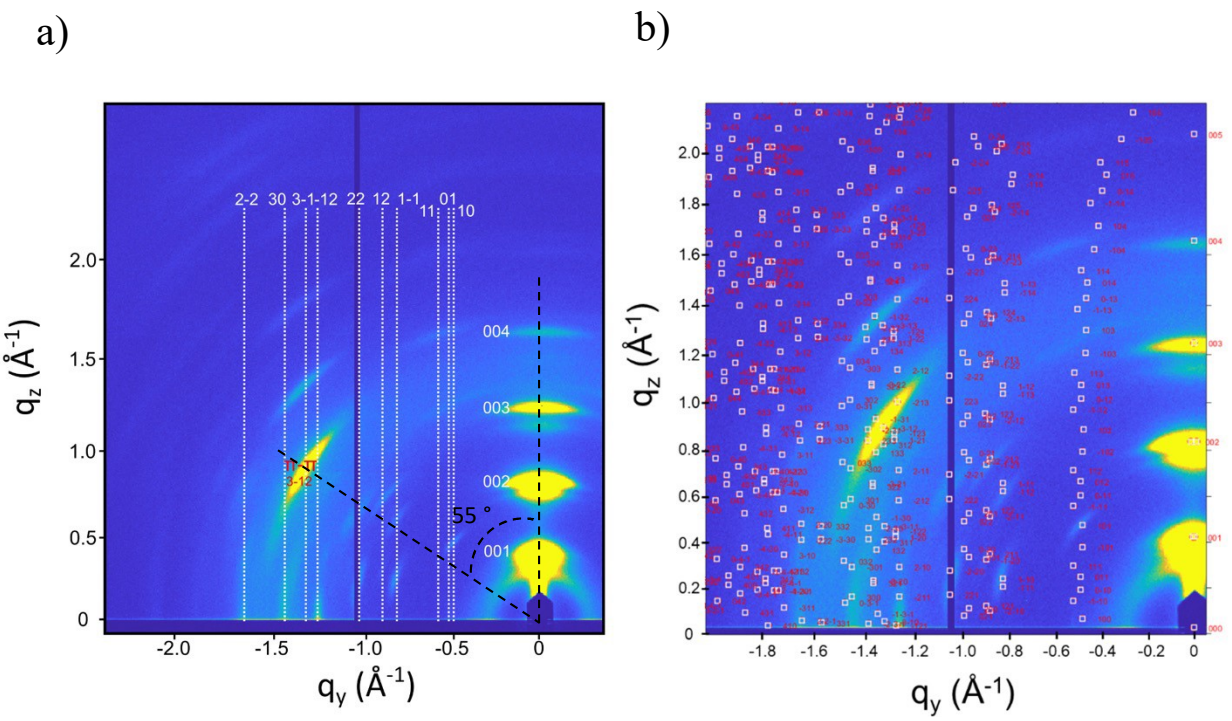

Figure S20. Indexing of the diffraction peaks from GIXD of the annealed films with the labeled Bragg rods (a, left) and full simulated diffraction pattern (b, right) with a P1 symmetry to show all possible peak positions.

Electrochemical and spectroelectrochemical characterization

Differential pulse voltammetry (DPV) and cyclic voltammetry (CV) were performed on glassy carbon electrodes (area: 0.07 cm^2). The glassy carbon electrodes were polished on polishing pads with Al_2O_3 slurries (1 µm, 0.1 µm, and 0.05 µm) to create a mirror finish and then rinsed with copious amounts of water. Films of TPT-TT were prepared via drop casting a one µL aliquot of a 2 mg/mL TPT-TT in chloroform solution. The electrolyte used for all electrochemical experiments was 0.5 M tetrabutylammonium hexafluorophosphate in propylene carbonate ($TBAPF_6$/PC). $TBAPF_6$ was purchased from Acros Organics (98%) and purified via recrystallization from hot

ethanol before use. The reference electrode was a Ag/Ag^+ pseudoreference electrode (inner solution: 10 mM $AgNO_3$ in 0.5 M $TBAPF_6$ in acetonitrile, calibrated versus Fc/Fc^+ that had an estimated $E_{1/2}$ of 0.08 V). The counter electrode was a Pt flag. DPV and CV were recorded using an EG&G PAR 273A potentiostat/galvanostat under CorrWare control between -0.5 V and 0.8 V vs Ag/Ag^+ (i.e., -0.58 and 0.72 V vs. Fc/Fc^+). The scan rate used for the cyclic voltammetry was 20 mV/s whereas the DPV used a step size of 2 mV, step time of 0.08 seconds, and a pulse amplitude of 20 mV. All experiments were conducted under an argon blanket in degassed electrolyte solutions.

The onset of oxidation is found to be 0.1 V vs. Fc/Fc^+, equivalent to an IE of 5.22 eV (assuming Fc/Fc^+ is -5.12 eV vs. vacuum). Using the optical band gap of 2.07 eV (thin-film onset of absorption of 600 nm, see Figure 2b) and making the crude assumption of neglecting any exciton binding energy, the electron affinity is estimated to be 3.15 eV.

The spectroelectrochemistry and solution doping experiments were carried out with an Agilent Cary 5000 spectrophotometer and 1 cm path length quartz cuvettes. For the spectroelectrochemistry, TPT-TT films were spray-coated to an optical density of ~ 1 from 4 mg/mL choloform solutions with an Iwata Eclipse HP-BC airbrush spray gun with an optimized argon pressure of 20 psi onto ITO coated glass slides (8-12 ohm/sq, Delta Technologies). The ITO/glass electrodes had been cleaned by sonication in sodium dodecyl sulfate/H_2O, H_2O, toluene, and finally isopropanol (IPA) prior to use. The films were cycled 10 times from -0.58 to 0.72 V vs. Fc/Fc^+ at 50 mV/s before recording a spectrum. The current and voltage were controlled and measured using an EG&G PAR 273A potentiostat/galvanostat. The films were held at the desired potential for 30 seconds before a spectrum was recorded. For the solution doping, TPT-TT was

dissolved at a concentration of 0.05 mg/mL in chloroform and Fe(III)tos dissolved at 10 mg/mL in dry acetonitrile was titrated into the TPT-TT solution in aliquots of 0.25 equivalents.

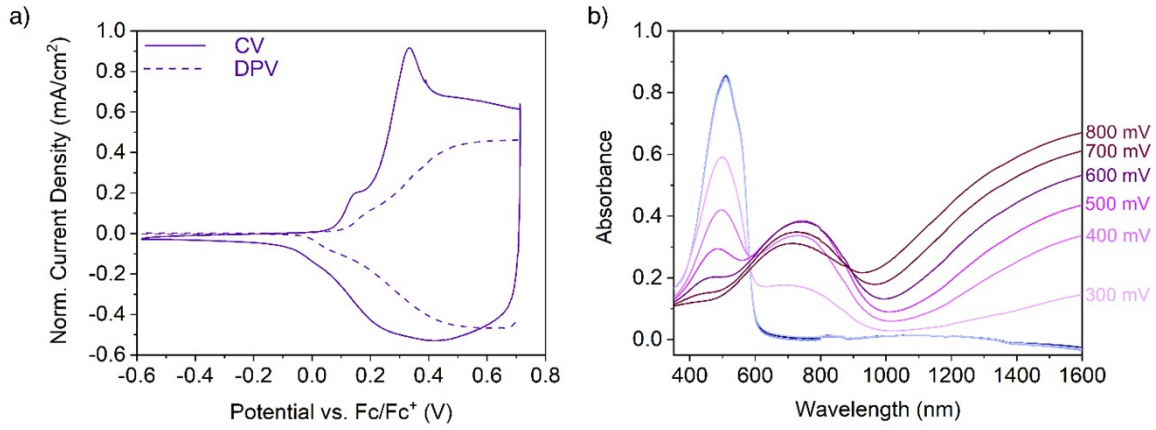

Figure S21. (a) Cyclic voltammetry (solid lines) and differential pulse voltammetry (dashed lines) of TPT-TT measured in degassed 0.5 M $TBAPF_6$/propylene carbonate. The films were prepared by drop casting from 2 mg/mL chloroform solutions onto glassy carbon electrodes. The cyclic voltammograms were recorded at 20 mV/s whereas DPV was measured with a step size of 2 mV, a step time of 0.08 seconds, and a pulse amplitude of 20 mV from -0.58 to 0.72 eV vs. Fc/Fc^+. (b) Potential dependent spectra of a TPT-TT film on ITO/glass in 0.1 V increments, demonstrating the bleaching of the π-π* of the neutral polymer as the film is electrochemically oxidized.

The spectroelectrochemistry results (Figure S17) provide strong support for the DPV results where depletion of the π-π* band at 513 nm initiates at ~0.1 V vs $Fc/Fc^{+\cdot}$ Simultaneously, we observe the emergence of charge carrier bands at 749 nm and beyond 1600 nm. Notably, the high-energy charge carrier band reaches its peak intensity at ~0.5 V vs Fc/Fc^+, followed by a

subsequent decrease in intensity accompanied by a blue-shift of the lower-energy charge carrier band. These findings collectively suggest the co-existence of radical cations and dications (polarons/bipolarons) in electrochemically doped TPT-TT.

Electrical conductivity, Seebeck coefficient, and doping procedures

TPT-TT was dissolved in HPLC-grade chloroform with a stir bar at a concentration of 15 mg/mL. The solution was heated to 35 °C and stirred to aid in dissolution. Glass microscope slides were prescored and diced into strips about 1 cm wide and 5-6 cm long. Slides were cleaned by sonication in sodium dodecyl sulfate/DI water, followed by rinse with DI water, and sonication in IPA. The slides were wiped clean with a Kim-wipe and blown with compressed air to remove dust. The slides were loaded onto a shadow mask and four platinum contact pads in a van der Pauw geometry were deposited via magnetron sputtering using a custom-built sputtering chamber.

Films were formed by blade coating using a blade height of 175 μm (Zehntner Testing Instruments, ZAA 2300). Approximately 10-15 μL of 35 °C solution was put down as a thin line with a room temperature pipette and immediately blade coated with a speed of 50 mm/s. The polymer-coated strips were broken into approximately 1 cm x 1 cm samples and vacuum dried at room temperature overnight. After vacuum drying, films were randomly selected and annealed in a glovebox by heating to 250 °C at 10 °C/min, then slowly cooled to room temperature.

Dopant solutions were prepared by dissolving iron(III) p-toluenesulfonate (ferric tosylate) at a 50 mM concentration in acetonitrile. The estimated LUMO of the dopant lies deeper in energy than the HOMO of TPT-TT, at -5.25 eV vs. vacuum, enabling spontaneous electron transfer from the HOMO of TPT-TT to the LUMO of the dopant. The dopant solutions were

prepared fresh and used immediately. 40 μL of dopant solution was drop-casted onto the TPT-TT films such that the area between the contact pads was completely covered. The films were then covered with a petri dish and left undisturbed for one minute. Then, the dopant solution was carefully pipetted off and the films were immersed in IPA to wash away any excess dopant salt. Films were then dried under vacuum for five minutes.

Electrical conductivity and Seebeck measurements were made with a custom setup. Micromanipulators with tungsten tips were used to gently pierce the film and make electrical contact to the bottom platinum contact pads. The in-plane electrical conductivity was acquired using the four-probe van der Pauw technique (Note: Pt contact pads were put under the polymer film, depositing Pt on the film surface resulted in incomplete doping under the contact pad and larger standard deviations). The Seebeck coefficient was measured by suspending the sample between two temperature-controlled Peltier units such that the center of the film between the contact pads was in the center of the gap (separated by 3 mm). The thermoelectric voltage was measured between two contact pads on separate stages using the probe tips, while the temperature of each pad was measured with a K-type thermocouple situated near the probe tips. A temperature difference of $\Delta T = 10$ K was applied to the film, and the resulting thermovoltage was measured. The Seebeck coefficient was calculated as the slope of the V vs ΔT plot. Voltage and temperature data were acquired using a Keithley 2700 DMM with a 7708 Mux card via a LabVIEW interface.

After transport measurements, the film thickness was measured with a Bruker DektakXT profilometer. A cut was made across the film in the direction of blade coating, then the average film thickness between the contact pads was measured in at least 2 different spots. Thicknesses were used to calculate corrected electrical conductivities.

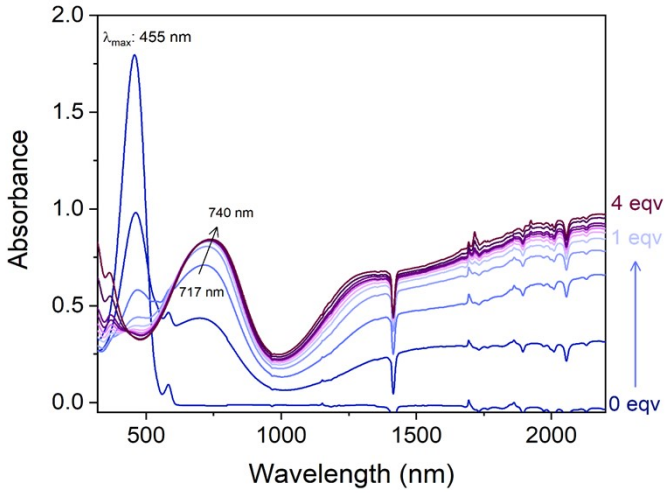

Figure S22. UV-vis-NIR spectra obtained during chemical doping of TPT-TT solution (0.05 mg/mL0 in $CHCl_3$) with 10 mg/mL solution of iron(III) p-toluenesulfonate (ferric tosylate) in acetonitrile added in 0.25 equiv. (relative to repeat unit) increments from 0 to 2 eq, then +1 equiv. until 4 equiv. where the depletion of the π-π* band is an indication of successful conversion of the neutral to the doped state.

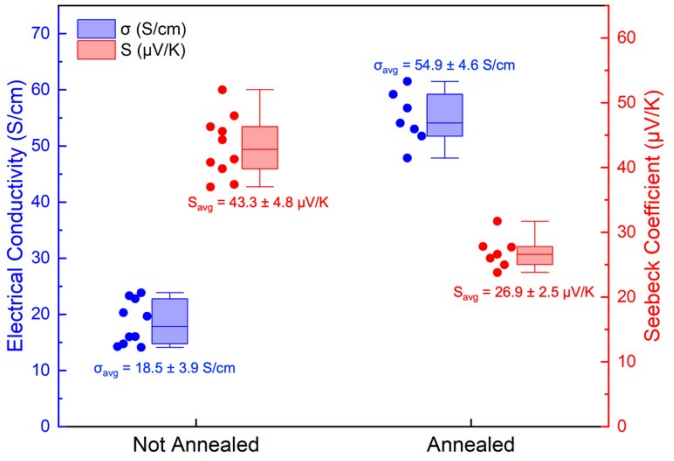

Figure S23. Electrical conductivity and Seebeck coefficient for as-cast and annealed TPT-TT films. Each individual point represents a measured film. Averages and sample standard deviations are annotated on the graph.

OFET device fabrication details

Device fabrication started with cleaning the substates in consecutive baths of warm acetone and warm IPA (85 °C), followed by UV-Ozone cleaning and a thorough DI water rinse and then drying under a stream of nitrogen. First, a bilayer of 3 nm Ti and 40 nm Au was deposited through a shadow mask to serve as source/drain contacts. The channel lengths *L* varied between 30 and 100 µm, while the channel widths *W* varied between 200 and 1000 µm. The contacts have been treated with pentafluoro benzene thiol (PFBT) to improve charge injection.[10] Next, the TPT-TT layer was deposited by spin coating it from a 1wt% solution in room temperature chlorobenzene, at a spinning speed of 1000 in a nitrogen glovebox. A set of films were annealed at 250 °C for 10 min in the same glovebox, then cooled slowly, while the other was used immediately after the spin-coating process. Without exposure to air, in the next step the polymer dielectric Cytop was spin coated at a spinning speed of 2000 rpm on top of TPT-TT, then cured in a vacuum oven at room temperature for about 12 h. The top gate electrode was then deposited through a shadow mask.

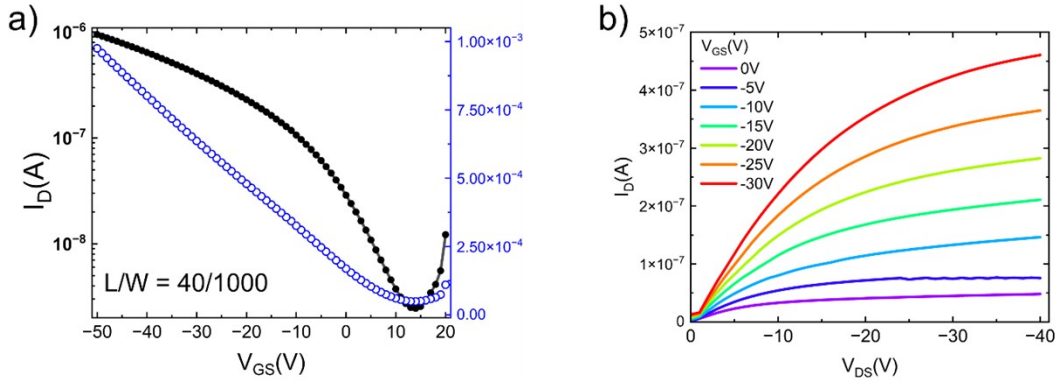

Figure S24. Electrical properties of TPT-TT transistors that have not been annealed. a) Transfer curve in the saturation regime (VDS = - 50 V) for a device that was annealed prior to testing, having L = 40 µm and W = 1000 µm. b) Output curves for the same device.

Space-charge-limited current (SCLC) measurements

The out-of-plane mobility of the TPT-TT thin-film was assessed using a hole-only device configuration of ITO/MoO_3/polymer/MoO_3/Ag within the space-charge limited regime. For the hole-only device fabrication, the patterned ITO glass substrates were sequentially cleaned for 15 min in detergent solution (2% Mucasol (Schülke)), deionized water, acetone (Sigma-Aldrich, ≥99.5%), and IPA (Fisher Chemical). ITO substrates were dried with N_2 gun and then subjected to a UV ozone treatment for 10 minutes. A 10 nm layer of MoO_3 was evaporated at a pressure of 10^{-6} torr using a shadow mask to make 8 independent pixels on a single substrate; the active area of each pixel is 0.07 cm^2. The TPT-TT polymer dissolved in chlorobenzene (concentrations of 20-35 mg/ml) was deposited via static spin coating at a speed of 1000 rpm for 60 seconds with a ramp rate of 5 seconds. To explore the thickness dependence of $J \sim 1/L^3$, four different concentrations of TPT-TT solutions were utilized: 20 mg/ml, 25 mg/ml, 30 mg/ml, and 35 mg/ml. Subsequently, TPT-TT thin films were annealed at 250 °C and then gradually cooled to room temperature. Then, a layer of MoO_3 (10 nm) followed by 100 nm of Ag were evaporated at a pressure of 10^{-6} torr on the active layer to obtain the completed devices. Fast-drying Ag paint (Ted Pella, 16040-30) was applied to the ITO electrodes to improve contacts with the device switch box. J-V characteristics were recorded with Keithley 2410 SourceMeter® SMU under dark conditions. Resulting J-V curves, mobility fits, and thickness dependence verifications for the annealed TPT-TT films as well as un-annealed films are shown below. TPT-TT solution preparation, spin-coating, evaporation, and J-V measurement were all done under Ar_2 atmosphere inside the glovebox. Hole mobility was extracted using the Mott-Gurney Law. The detailed equation for fitting and analysis process follows the previously reported literature.[11]

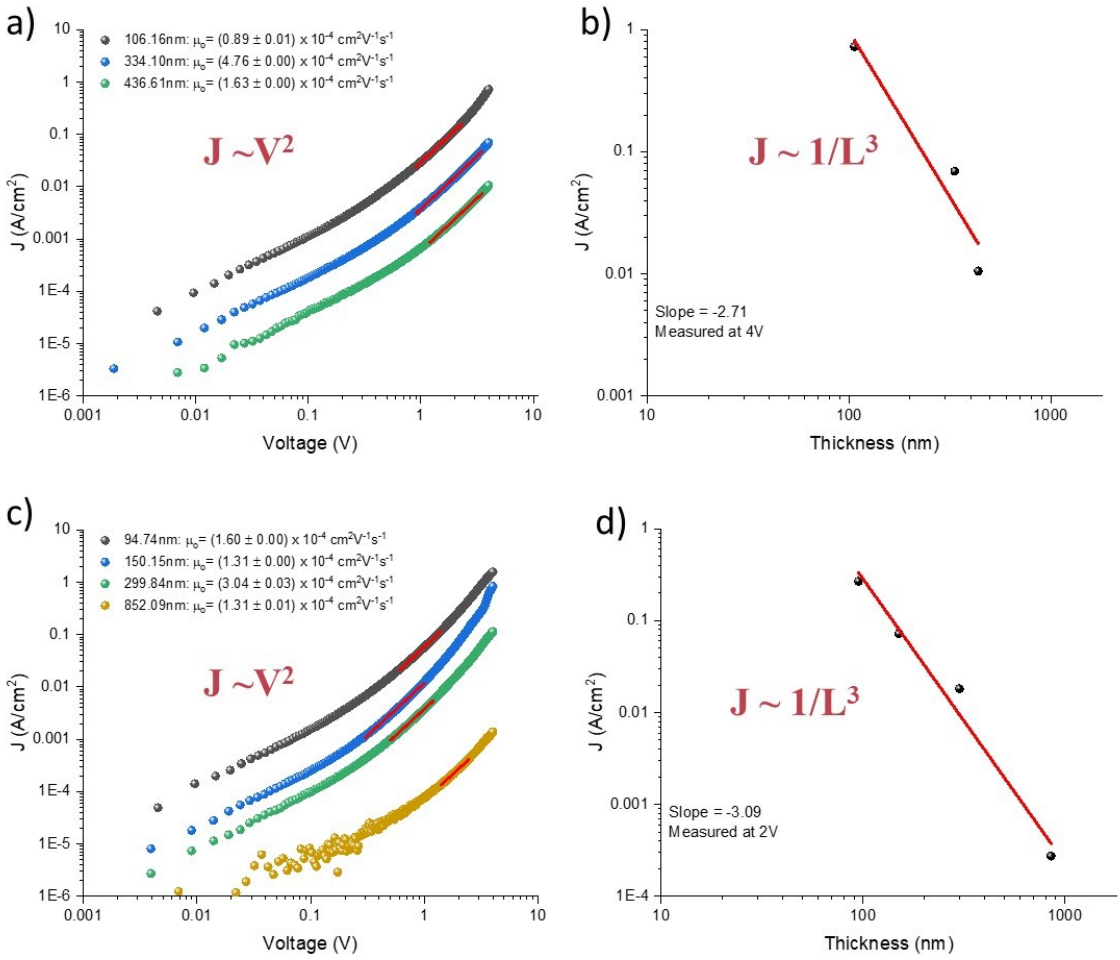

Figure S25. J-V curves and mobility fits (a), and thickness dependence checks (b) for un-annealed samples. Data for the annealed samples are shown in (c, J-V curves and mobility fits) and (d, thickness dependence checks) in SCLC regime hole-only mobility measurements for TPT-TT.

References

1. Gaussian 16, Revision C.01, M. J. Frisch, G. W. Trucks, H. B. Schlegel, G. E. Scuseria, M. A. Robb, J. R. Cheeseman, G. Scalmani, V. Barone, G. A. Petersson, H. Nakatsuji, X. Li, M. Caricato, A. V. Marenich, J. Bloino, B. G. Janesko, R. Gomperts, B. Mennucci, H. P. Hratchian, J. V. Ortiz, A. F. Izmaylov, J. L. Sonnenberg, D. Williams-Young, F. Ding, F. Lipparini, F. Egidi, J. Goings, B. Peng, A. Petrone, T. Henderson, D. Ranasinghe, V. G. Zakrzewski, J. Gao, N. Rega, G. Zheng, W. Liang, M. Hada, M. Ehara, K. Toyota, R. Fukuda, J. Hasegawa, M. Ishida, T. Nakajima, Y. Honda, O. Kitao, H. Nakai, T. Vreven, K. Throssell, J. A. Montgomery, Jr., J. E. Peralta, F. Ogliaro, M. J. Bearpark, J. J. Heyd, E. N. Brothers, K. N. Kudin, V. N. Staroverov, T. A. Keith, R. Kobayashi, J. Normand, K. Raghavachari, A. P. Rendell, J. C. Burant, S. S. Iyengar, J. Tomasi, M. Cossi, J. M. Millam, M. Klene, C. Adamo, R. Cammi, J. W. Ochterski, R. L. Martin, K. Morokuma, O. Farkas, J. B. Foresman, and D. J. Fox, Gaussian, Inc., Wallingford CT, 2016.

2. Plimpton, S.,. *Journal of computational physics*, 1995, **117(1)**, pp.1-19.

3. Jorgensen, W.L. and Tirado-Rives, J., *Journal of the American Chemical Society*, 1988, **110(6)**, pp.1657-1666.

4. Dodda, L.S., Cabeza de Vaca, I., Tirado-Rives, J. and Jorgensen, W.L., *Nucleic acids research*, 2017, **45(W1)**, pp.W331-W336.

5. Marenich, A.V., Jerome, S.V., Cramer, C.J. and Truhlar, D.G., *Journal of chemical theory and computation*, 2012, **8(2)**, pp.527-541.

6. Hockney, R.W. and Eastwood, J.W., 2021. Computer simulation using particles. crc Press.

7. Sato, S., Hashimoto, K. and Tajima, K., *Synthetic metals*, 2011, **161(13-14)**, pp.1289-1298.

8. Wu, C.S. and Chen, Y. *Journal of Polymer Science Part A: Polymer Chemistry*, 2010, **48(24)**, pp.5727-5736.

9. Feng, Y., Das, P.J., Young, R.M., Brown, P.J., Hornick, J.E., Weber, J.A., Seale, J.S., Stern, C.L., Wasielewski, M.R. and Stoddart, J.F., *Journal of the American Chemical Society*, 2022, **144(37)**, pp.16841-16854.

10. Waldrip, M., Jurchescu, O.D., Gundlach, D.J. and Bittle, E.G.,. *Advanced Functional Materials*, 2020, **30(20)**, p.1904576.

11. Advincula, A.A., Pelse, I. and Reynolds, J.R., *Journal of Materials Chemistry C*, 2020, **8(46)**, pp.16452-16462.